



41134
470575

TECHNICAL MEMORANDUM

X-151

MIXING CHARACTERISTICS DOWNSTREAM OF CORE REGION OF HIGH-
TEMPERATURE AXISYMMETRIC JETS EXHAUSTING INTO
TRANSONIC AND SUPERSONIC STREAMS

By Ronald G. Huff and Kaleel L. Abdalla

Lewis Research Center
Cleveland, Ohio

Declassified April 23, 1962

NATIONAL AERONAUTICS AND SPACE ADMINISTRATION
WASHINGTON

March 1960

NATIONAL AERONAUTICS AND SPACE ADMINISTRATION

TECHNICAL MEMORANDUM X-151

MIXING CHARACTERISTICS DOWNSTREAM OF CORE REGION OF HIGH-
TEMPERATURE AXISYMMETRIC JETS EXHAUSTING INTO
TRANSONIC AND SUPERSONIC STREAMS*

By Ronald G. Huff and Kaleel L. Abdalla

SUMMARY

A series of rocket motors with varying exit to throat area ratios was tested in the 8- by 6-foot wind tunnel to determine the effects of mixing on jet diameter and temperature decay at large distances ($x/d > 30$) from the nozzle exit. An approximate method to account for effects of the initial expansion was evolved. It was determined that the combustion efficiency has an important effect on jet spreading, since the unburned products can burn downstream of the nozzle. The data showed considerable scatter; however, mixing rates were, in general, lower than those observed for subsonic jets. Data for angles of attack of 5° and 10° are also presented, giving the respective centerline shift and temperature decay as a function of axial distance.

INTRODUCTION

Supersonic jet-spreading rates and temperature distributions at large distances downstream of the nozzle exit are of importance to aircraft and missile designers for problems such as jet infrared radiation and engine inlet ingestion of exhaust products from airborne rockets. "Large distances downstream" means distances on the order of those required for elimination of the central potential core in the jet. The shear region extends across the entire jet, and mixing profiles at successive stations are essentially similar.

The general case is complicated by the fact that the jet issues initially from a nozzle having a nonzero exit angle into a region of different static pressure. Studies of jet spreading in the region near the nozzle exit (see refs. 1 and 2, e.g.) have shown that the process of pressure- and flow-direction equalization can have a much greater effect on initial jet-spreading rates than the mixing process.

The size of the jet and the spreading rate at large downstream distances will then depend on two independent processes: first, the pressure-direction equalization that rapidly changes jet size near the nozzle, and second, the more gradual mixing of the equalized jet and the surrounding stream at constant pressure.

Available data on spreading rates near the nozzle show that the problem is complicated, and the data are not sufficient to obtain effective jet size after equalization as a function of body-nozzle geometry, jet pressure ratio, stream Mach number, and so forth. Suitable information on mixing is likewise lacking. Although considerable theoretical and experimental work has been done with subsonic jets and streams (see, e.g., refs. 3 and 4), supersonic spreading rates as a function of velocity and density ratios between jet and stream are not available.

The primary objectives of the present investigation were to obtain spreading and temperature distribution data for hot supersonic jets exhausting into high-speed streams (Mach 0.8 to 2.0) and to show the effect of the initial expansion on these downstream spreading characteristics. A secondary objective was to develop a simple method that, with the use of existing information on free jet expansion, would provide approximate answers for spreading rates.

Three small rocket motors having a nominal thrust of 250 pounds and of varying exit to throat area ratio were used to produce the hot supersonic jets. The motors used JP-LOX at a stoichiometric fuel-oxygen ratio and were tested in the 8- by 6-foot supersonic wind tunnel at stream Mach numbers from 0.8 to 2.0. The basic data were obtained at an angle of attack of zero; angles of 5° and 10° were investigated briefly. A total-temperature rake was used to survey the flow.

SYMBOLS

A	area
c^*	characteristic velocity
d	diameter
$d_{0.5}$	"half" diameter of the jet; diameter at which temperature equals $(T_m + T_0)/2$
F,G	Mach number functions
g	acceleration due to gravity, 32.174 ft/sec^2
M	Mach number

M	molecular weight
O/F	oxidant-fuel mass ratio
P	total pressure
p	static pressure
R	universal gas constant
Re	Reynolds number per foot
r	radius
T	total temperature, °R
T_{\max}	maximum total temperature in jet at a given station
V	velocity
w	total flow rate into rocket motor (LOX, JP-4 weight flows)
x	axial distance from nozzle exit
y_{ξ}	local jet centerline displacement due to angle of attack
α	angle of attack, deg
γ	ratio of specific heats
η	combustion-efficiency parameter, T_c/T'_c
θ	$(T_2 - T_c)/(T'_c/T_c) = (\tau - 1)/[1/(\eta - 1)]$
λ	ratio of free-stream velocity to equalized jet velocity, V_0/V_2
λ_{adj}	value of λ_{eff} for which temperature and spreading data agree
λ_{eff}	effective low-speed value from fig. 5
ρ	density
τ	afterburning parameter, $\frac{T_2}{T_1} = \frac{T_2}{T_c}$
τ_{adj}	value of τ for which temperature and spreading data agree

Subscripts:

ξ	jet centerline, point in jet where maximum temperatures exist
c	combustion chamber
e	nozzle-exit station
max	maximum
min	minimum
t	rocket throat station
0	free-stream conditions
1	station at which jet is fully expanded
2	station at which burning ceases and mixing begins

Superscript:

'	denotes theoretical combustion-chamber conditions
---	---

APPARATUS AND PROCEDURE

The rocket motors used were water-cooled and utilized JP-4 and LOX as the rocket propellant. A sketch of motor and model details is shown in figure 1. The three nozzle-afterbody combinations that were tested are sketched in figure 2. All nozzles were conical with a 15° half-angle and had a throat diameter of 0.5 inch. The area ratios, A_e/A_t , were 3.44, 6.25, and 18.31. The base size and the boattail angle were the minimum values consistent with the motor structural and cooling requirements. The motors were mounted in the supersonic test section of the NASA Lewis 8- by 6-foot transonic-supersonic wind tunnel. Angles of attack up to 10° were possible and could be obtained without changing the location of the nozzle exit.

Figure 3 shows a sketch of the total-temperature survey rake and its mounting mechanism as installed in the transonic portion of the tunnel. The sting support strut is shown in the fore position. It was used as a steady rest and was moved to a position aft of the sting mounting strut for far-downstream rake locations. For each test the rake was traversed as far upstream as consistent with the maximum permissible rake temperature of 2000° F. The rake was so aligned as to measure the upper half of the jet profile at zero angle of attack. Rake thermocouples were spaced at 0.25 inch over the lower 4 inches (near the jet centerline); for the remainder, spacing was 1.0 inch.

Propellant flow rates were adjusted to obtain chamber pressures (nominal) of 300, 400, and 480 pounds per square inch. LOX to JP-4 ratio was held at stoichiometric ($O/F = 3.4$). Nominal tunnel test conditions at which each motor was run are given in the following table:

Mach number, M_0	Static press., P_0 , lb/sq in. abs	Total press., P_0 , lb/sq in. abs	Total temp., T_0 , $^{\circ}R$	Reynolds number per ft, Re_0
0.8	9.48	14.45	586	3.64×10^6
1.5	5.11	18.75	633	4.65×10^6
2.0	3.15	24.65	674	4.78×10^6

Instrumentation and Data-Recording Procedure

Rocket chamber pressure P_c was recorded on a pressure transducer. The fuel and LOX weight flows were recorded using turbine-type flowmeters. Chromel-Alumel thermocouples were used on the jet temperature survey rake and were of the shielded aspirating type (see fig. 3). One thermocouple of this type was placed on each side of the rake at approximately the horizontal jet centerline. These showed fairly good rake alinement.

Chamber pressure, JP-4 and LOX weight flows, and one scan of the rake temperatures were recorded as soon as the rocket motor had reached steady-state operation. Then, as the rake was moved upstream in steps, only the rake temperatures were recorded.

Data Reduction

Rocket motor parameters were obtained as follows. The theoretical characteristic velocity was computed from

$$(c^*)' = \frac{\sqrt{\frac{g \gamma_c' R T_c'}{\mathcal{M}_c'}}}{r' \left(\frac{2}{\gamma_c' + 1} \right)^{\frac{\gamma_c' + 1}{2(\gamma_c' - 1)}}} \quad (1)$$

where γ_c' , T_c' , and \mathcal{M}_c' were obtained from reference 5 for the proper values of P_c and O/F . The actual characteristic velocity was computed from

$$c^* = \frac{g P_c A_t}{w} \quad (2)$$

Combustion efficiency and chamber temperature could then be obtained from

$$\eta = [c^*/(c^*)']^{\zeta} \quad (3)$$

and

$$T_c = \eta T_c' \quad (4)$$

The values of P_c/p_e and γ_e were obtained by plotting the tabulated values of reference 5 as a function of area ratio A_e/A_t . The value of the exit Mach number M_e was then obtained from

$$M_e = \sqrt{\frac{2}{\gamma_e - 1} \left[(P_c/p_e)^{\frac{\gamma_e - 1}{\gamma_e}} - 1 \right]} \quad (5)$$

The measured rake voltages were converted to temperatures, and these temperatures were used directly to compute the temperature ratio $(T - T_0)/(T_{\max} - T_0)$. (Calibrations of similar thermocouples have shown recovery factors of 0.99+.)

The half diameter $d_{0.5}$ was calculated as twice the distance between the thermocouple having the maximum temperature and that having a temperature equal to $(T_{\max} + T_0)/2$.

STATEMENT OF PROBLEM AND METHOD OF ATTACK

Equalization

Although the object of the investigation is to study fully developed supersonic mixing rates, the pressure- and flow-direction process that occurs near the nozzle exit is of direct concern, since it can result in large changes in the size of the jet and hence in the scale of the mixing process. The complexities of equalization are illustrated in figure 4(a).

The jet and the stream first expand into base region in which the pressure is usually below ambient. Both streams next pass through a series of shocks and expansions that simultaneously turn the flow toward the axial direction and adjust the static pressure to ambient. Mixing starts in the base region. The initial boundary-layer velocity profiles are altered first by the expansion at the base, next by the mixing with the semidead air in the base region, and again as the flow passes through the trailing shock and the succeeding expansions and shocks. An added factor is the possibility of burning within the jet downstream of the nozzle exit.

In the region close to the nozzle exit, jet-spreading rates are then a complicated function of the equalization process and the mixing along the boundary. Fortunately, if the shocks and expansions are strong, the process is essentially complete within 2 to 3 diameters of the exit (see, e.g., the schlieren photographs of ref. 1), so that the major part of the mixing process must occur essentially at constant pressure. Therefore, if an estimate of the effective diameter of the jet at the completion of pressure- and flow-direction equalization can be obtained, it may be possible to correlate spreading data obtained at different jet pressure ratios and/or with different nozzles and, in addition, to correlate the present data with existing low-speed data of reference 4.

Idealized Model

The actual equalization process is far too complicated to generalize; however, for the idealized case of figure 4(b) the effective diameter at the start of mixing can be obtained.

For simplicity, the equalization process is taken in two steps. In the first, the pressure-direction equalization region (between stations e and 1), the jet expands freely to the ambient pressure p_0 . Interactions between jet and stream as well as mixing and heat transfer along the boundary are neglected. The second region (between stations 1 and 2) is included in the idealized process so that any burning that occurs downstream of the nozzle exit can be accounted for. The afterburning is assumed to occur at ambient pressure. Downstream of station 2 the two uniform parallel streams start to mix at constant pressure. The region of interest in the present investigation is, of course, downstream of station 2 where the mixing has progressed to the jet center and the constant-velocity core has been eliminated.

The procedure used to calculate quantities at stations 1 and 2 was first to obtain the diameter d_1 from the characteristic solution of reference 6. (Details are in the appendix; results for each run are in table I.) The Mach number M_1 and the stream-jet velocity ratio λ were then calculated using jet mass-flow continuity.

The proper value of the afterburning temperature ratio was, of course, not known beforehand. However, for each assumed afterburning ratio, $\tau \equiv T_2/T_c$, the diameter d_2 could be calculated using the one-dimensional continuity and momentum relations. (As shown in the appendix, the velocity ratio is unchanged by afterburning.) Several values were assumed, and the proper value was obtained from data analysis, as will be discussed more fully after the data are presented.

Low-Speed Data

The results of reference 4 on the constant-pressure mixing of coaxial streams include velocity ratios in the range of interest for the present investigation and were therefore used for comparison. Actually the tests were run with cold jets ($T_0/T_c \approx 1$), and the spreading characteristics were obtained by measuring the rate at which helium in the jet mixed with the stream. However, as discussed in reference 4, experimental evidence indicates that mass and temperature spread at essentially equal rates for turbulent mixing.

Curves obtained by cross-plotting the data of reference 4 and assuming that temperature ratio could replace helium concentration are presented in figure 5. Also included is a sketch illustrating the terminology. Jet parameters at the start of mixing are d_2 , T_2 , and V_2 . At any axial station, T_{\max} is the maximum local temperature and $d_{0.5}$ is defined as the diameter for which the temperature is above ambient (or below T_{\max}) by half of the local maximum increment. Since the best fit to the temperature profile data is a cosine curve, it can be seen that $d_{0.5}$ is also the "half diameter" of the jet.

In the section that follows, the present data are compared with the curves of figure 5. The effects of stream-jet density ratio and the absolute magnitude of velocity (compressibility effects) should show up as discrepancies.

RESULTS AND DISCUSSION

Zero Angle of Attack

Temperature profiles. - The temperature profiles were normalized by plotting $(T - T_0)/(T_{\max} - T_0)$ against $r/r_{0.5}$, where $r_{0.5}$ is the "half" radius. The shaded area representing data for all nozzles and over the pressure-ratio and axial-distance ranges tested is compared in figure 6 with an empirical cosine relation that was found to give good agreement in reference 4. It can be seen that the cosine variation falls close to the center of the shaded region except near the outer edge of the mixing region.

Jet spreading. - For the spreading data of figure 7, both the half diameter $d_{0.5}$ and the axial distance x are expressed as ratios of the calculated diameter after equalization d_2 . As has been explained, the use of d_2 is an attempt to account for the initial expansion. Zero afterburning was assumed ($\tau = 1$), so that $d_2 = d_1$. The pertinent

parameters for each run are listed. (Additional information is listed in table I.) Also included are the curves of figure 5.

In figure 7, many of the data sets have slopes that are in good agreement with the curves for the low-speed data. A large number have near zero slope, however, and no reasonable explanation for this result is apparent. In general, if the present data are compared with the curve having the same velocity ratio, the present data indicate lower spreading rates. However, if, as has been mentioned previously, density differences between jet and stream affect mixing rates, the present data and the curves should not be compared at the same λ .

Temperature decay. - An additional possibility for the discrepancies becomes evident from the maximum (centerline) temperature distributions of figure 8. The temperature ratio $(T_{\max} - T_0)/(T_2 - T_0)$ is plotted as a function of x/d_2 assuming no afterburning ($T_2 = T_c$ and $d_2 = d_1$). Comparison with the low-speed curves again indicates either lower average spreading rates (i.e., higher temperatures) or the need for different λ values. An important additional point, however, is the fact that the temperature ratio exceeds unity by large amounts for the low-combustion-efficiency runs. It is clear that the unburned fuel must burn downstream of the throat and that as a result of the afterburning the effective temperature at the start of mixing T_2 must in some cases be greater than the combustion temperature T_c .

Afterburning and velocity ratios. - Three possibilities for the discrepancies between the low-speed, constant-density data and those of the present investigation have been mentioned:

- (1) Afterburning, which changes the effective temperature and jet diameter at the start of mixing
- (2) Density differences between jet and stream, which can change mixing rates
- (3) Differences in velocity magnitudes

An additional possibility, of course, is that the computation for the effective diameter after expansion is not sufficiently sophisticated. However, for runs 9 and 10 the jet exit pressure ratio p_e/p_0 is close to unity (see table I), and it is probable that the diameter ratio d_1/d_e cannot be greatly in error. For runs 9 and 10, then, one or more of the three preceding faults must exist.

The data of figure 8 show that afterburning is more than a possibility; the problem is that the proper amount of afterburning is not

known a priori. The problem was handled by using a technique in which an afterburning ratio ($\tau = T_2/T_c$) was assumed. The diameter d_2 was then computed; the quantities x/d_2 , $d_{0.5}/d_2$, and $(T_{\max} - T_0)/(T_2 - T_0)$ were obtained; and the data were replotted. The results were superimposed on the curves of figure 5, and effective low-speed velocity ratios were read off for both the spreading data and the temperature data. The process was then repeated for a different assumed afterburning ratio.

Typical results of the procedure are presented in figure 9. Effective low-speed velocity ratio λ_{eff} is plotted as a function of assumed afterburning ratio for the data of run 10. It can be seen that, as afterburning ratio increases, the effective velocity ratio increases for the spreading data and decreases for the temperature data. Moreover, the afterburning ratio for which λ_{eff} equals the actual λ is different for the temperature data ($\tau = 2.9$) and for the spreading data ($\tau < 1.0$). There does exist, however, an afterburning ratio for which both data sets are satisfied. For run 10 the "adjusted" values are $\tau_{\text{adj}} = 2.46$ and $\lambda_{\text{adj}} = 0.44$, and the velocity-shift ratio $\lambda_{\text{adj}}/\lambda$ is 1.91.

A summary of adjusted values is included in table I and is also shown in figure 10, where both ratios are plotted as functions of combustion efficiency. The symbols indicate stream Mach number (symbol shape), jet exit pressure ratio (tail location), and nozzle area ratio (solid or open). Also included are curves of constant $\theta = (T_2 - T_c)/(T_c' - T_c)$. The numerator is the afterburning temperature increase; for stoichiometric O/F (3.403), the denominator is a measure of the maximum possible increase. The value of θ is therefore essentially the ratio of actual to maximum temperature rise for all data except that of run 7 ($O/F = 2.73$).

The velocity-shift-ratio data show a scatter that has no definite trend with either stream Mach number, pressure ratio, area ratio, or combustion efficiency. Most points fall within $\lambda_{\text{adj}}/\lambda = 1.5 \pm 0.3$, thus indicating definitely lower mixing rates than would have been determined using the calculated velocity ratio λ and figure 5. The afterburning results show that, independent of nozzle type and operating conditions, the temperature rise is about half of the maximum value.

Using an uncertainty in velocity-shift ratio of ± 0.3 with the curves of figure 5, the situation in supersonic hot jet mixing can be summarized as follows: With the simple approximation for the effect of initial expansion and using a velocity-shift ratio of 1.5 on the curves of figure 5, the resulting jet size and temperature will be within ± 18 percent for x/d_2 less than 100. Whether density or compressibility effects are responsible for the lower mixing rates is not known.

Angle of Attack

Because of the limited amount of angle-of-attack data obtained, extensive analysis was not made. The discussion is limited to presentation of the results and observations of the major trends.

Centerline shift. - Shift variations with angle of attack, jet pressure ratio, and stream Mach number are plotted in figure 11. Centerline shift is expressed as a fraction of the effective diameter d_1 . From figure 11(a), it can be seen that increasing Mach number decreases the offset ratio despite the fact that a pressure-ratio increase accompanies the Mach number increase. For the larger-area-ratio nozzle, however, offset ratio is almost independent of Mach number (compare figs. 11(b), (c), and (d)). For the range of variables investigated, shift ratios were approximately 1 for 5° angle of attack and 2 for 10° .

Mixing properties. - In figures 12 and 13 are shown the effects of angle of attack on mixing characteristics. It is apparent from figure 12 that the spread of the jet, in the vertical test plane (no measurements of jet spreading were taken in the plane normal to the vertical plane), is not appreciably affected by angle of attack. On the other hand, figure 13 shows that angle of attack definitely decreases the jet maximum temperature.

Unfortunately, most of the data in figures 12 and 13 are for over-expanded nozzles ($p_e/p_0 < 1.0$). However, the data in figures 12(a) and 13(a) at Mach numbers of 1.5 and 2.0 are for underexpanded nozzles. These data agree with the preceding conclusion. It should be noted, however, that the differences of jet maximum temperature with angle of attack are smaller if the nozzle is overexpanded.

SUMMARY OF RESULTS

The following conclusions on downstream mixing are drawn from the results of a test conducted in the NASA Lewis 8- by 6-foot wind tunnel using JP-4 and LOX as propellants in small rocket motors operated at various combustion efficiencies:

1. The jet temperature profiles at various axial distances were similar and approximated those obtained in existing subsonic data.
2. Mixing rates were lower than those for the low-speed cold jet data of reference 4.
3. Using a simplified method to account for the initial expansion, for afterburning, and for the lower mixing rate, the spreading and temperature decay data showed a scatter of ± 18 percent when compared with existing low-speed data.

4. Because of afterburning and the resulting change in effective jet size and temperature, combustion efficiency is an important parameter.

5. Angles of attack of 5° and 10° shift the jet centerline by approximately 1 and 2 jet diameters, respectively, at Mach 1.5. While the jet maximum temperature decreases with angle of attack, the spread of the jet remains nearly constant.

Lewis Research Center

National Aeronautics and Space Administration

Cleveland, Ohio, November 13, 1959

APPENDIX - METHOD USED TO CALCULATE JET CONDITIONS

AT STATION WHERE JET AFTERBURNING CEASES

Mach number functions that will be useful in the derivations that follow are:

$$F = \sqrt{\left(\frac{2}{\gamma+1}\right)^{\frac{\gamma+1}{\gamma-1}}} \frac{1}{M \sqrt{1 + \frac{\gamma-1}{2} M^2}}$$

and

$$G = \sqrt{\gamma} \frac{M}{\sqrt{1 + \frac{\gamma-1}{2} M^2}} = V \sqrt{\frac{\gamma}{gRT}}$$

Charts of F and G as functions of M were prepared for several values of γ .

From flow continuity between the nozzle throat and station 1 and assuming $T_1 = T_c$ and $P_1 = P_c$,

$$A_1 \sqrt{\gamma_1} M_1 P_0 M_1 \sqrt{1 + \frac{\gamma_1 - 1}{2} M_1^2} = A_t \sqrt{\gamma_t} M_t \sqrt{\left(\frac{2}{\gamma_t + 1}\right)^{\frac{\gamma_t + 1}{\gamma_t - 1}}} P_c$$

Then

$$F_1 = \frac{P_0 A_1}{P_c A_t} \sqrt{\frac{\gamma_1 M_1}{\gamma_t M_t}} \left[\frac{\left(\frac{2}{\gamma_1 + 1}\right)^{\frac{\gamma_1 + 1}{\gamma_1 - 1}}}{\frac{\gamma_t + 1}{\left(\frac{2}{\gamma_t + 1}\right)^{\frac{\gamma_t + 1}{\gamma_t - 1}}}} \right] \quad (A1)$$

In the area ratio A_1/A_t , A_1 was assumed to be the maximum area in a free expansion. Numerical values were obtained as functions of P_c/p_0 and M_c from the characteristic solutions of reference 6. The bracketed term on the right in equation (A1) was neglected, since, for the maximum pressure ratio tested ($P_c/p_0 = 150$), it differs from unity by less than 1 percent. Mach number M_1 was found from equation (A1) and the curves of F against M .

For the assumed constant-pressure afterburning between stations 1 and 2 ($P_1 = P_2 = P_0$), equations can be written for conditions at station 2 as follows:

$$\text{Continuity: } \rho_1 V_1 A_1 = \rho_2 V_2 A_2$$

$$\text{Momentum: } (\rho_1 V_1 A_1) V_1 = (\rho_2 V_2 A_2) V_2$$

Obviously,

$$V_1 = V_2 \quad (\text{A2})$$

From equation (A2) and the definition of G ,

$$G_2 = \sqrt{\frac{T_c}{T_2}} \sqrt{\frac{M_2}{M_1}} G_1 \quad (\text{A3})$$

The Mach number M_2 can then be found from the G against M curves for any assumed value of afterburning temperature ratio $\tau = T_2/T_c$.

Finally, the jet diameter at station 2 can be found by rewriting the momentum equation:

$$\gamma_1 M_1^2 A_1 = \gamma_2 M_2^2 A_2$$

or

$$\frac{d_2}{d_1} = \frac{M_1}{M_2} \sqrt{\frac{\gamma_1}{\gamma_2}} \quad (\text{A4})$$

The ratio of the stream to jet velocity λ at stations 1 or 2 was obtained from

$$\lambda = \frac{V_0}{V_1} = \sqrt{\frac{T_0}{T_c}} \sqrt{\frac{M_1}{M_0}} \frac{G_0}{G_1} \quad (\text{A5})$$

REFERENCES

1. Rousso, Morris D., and Baughman, L. Eugene: Spreading Characteristics of a Jet Expanding from Choked Nozzles at Mach 1.91. NACA TN 3836, 1956. (Supersedes NACA RM E51LL19.)
2. Tatro, Robert E.: The Spreading Characteristics of Choked Jets Exhausting into a Supersonic Stream. TR-55-2, Arnold Eng. Development Center, Oct. 1955. (Contract AF-40(600)-620.)

3. Squire, H. B., and Trouncer, J.: Round Jets in a General Stream. R. & M. No. 1975, British ARC, Jan. 1944.
4. Forstall, Walton, Jr., and Shapiro, Ascher H.: Momentum and Mass Transfer in Coaxial Gas Jets. Meteor Rep. No. 39, Dept. Mech. Eng., M.I.T., July 1949. (Bur. Ord. Contract NOrd 9661.)
5. Huff, Vearl N., and Fortini, Anthony: Theoretical Performance of JP-4 Fuel and Liquid Oxygen as a Rocket Propellant. I - Frozen Composition. NACA RM E56A27, 1956.
6. Love, Eugene S., Woodling, Mildred J., and Lee, Louise P.: Boundaries of Supersonic Axisymmetric Free Jets. NACA RM L56G18, 1956.

TABLE I. - ROCKET-MOTOR OPERATING CONDITIONS AND PARAMETERS

d_e , in.	Ae/At	Pc/Pe	MO	Pc, lb/sq in. abs	Rake location	Pe/PO	Tc, OR	γ	Tc, OR	d _l /de	M _l (Assume $\gamma = 1.3$)	λ	τ_{adj}	λ_{adj}	$\frac{\lambda_{adj}}{\lambda}$	Run
0.325	3.44	20	0.8	300	Aft	1.582	6300	0.546	3440	1.41	2.09	0.19	1.45	0.31	1.63	1
				400	↓	2.110	6420	.531	3410	1.63	2.10	.19	1.52	.31	1.63	2
				480		2.560	6560	.386	2540	1.84	2.06	.22	1.73	.35	1.59	3
			1.5	300	Aft	2.905	6300	0.761	4794	2.24	1.66	0.31	1.05	0.435	1.405	4
				400	↓	3.915	6420	.781	5010	2.64	1.62	.31	-----	-----	-----	5
				530		5.185	6677	.840	5610	2.99	1.59	.30	.99	.36	1.20	6
1.25	6.25	47	0.8	400	Aft	6.355	6420	0.709	4552	3.41	1.58	0.41	0.968	0.78	1.90	7
				300	Aft } Fore }	0.674	6300	0.189	1191	1.03	2.14	0.31	{3.65 3.20	0.533 .40	1.72 1.29	8 8f
				400	Aft } Fore }	0.898	6420	0.257	1650	1.14	2.26	0.26	{2.65 3.23	0.46 .36	1.77 1.38	9 9f
2.14	18.31	202	0.8	480	Aft } Fore }	1.077	6580	0.291	1915	1.24	2.36	0.23	{2.46 2.37	0.44 .414	1.91 1.80	10 10f
				470	Aft	1.958	6575	0.298	1960	1.89	2.02	0.43	2.0	0.55	1.28	11
				300	Aft } Fore }	2.027	6300	0.255	1607	1.83	2.07	0.58	2.44	0.875	1.51	12
2.14			1.5	430	↓	2.902	6566	.311	2042	2.14	2.03	.52	1.78	.94	1.80	13
				480		3.245	6580	.322	2119	2.43	1.99	.52	1.77	.85	1.635	14
				300	Fore	0.1567	6420	0.570	3660	0.82	1.34	0.26	-----	-----	-----	16f
2.14			1.5	400	Aft	0.3876	6300	0.595	3750	1.00	1.98	0.31	1.31	0.555	1.79	15

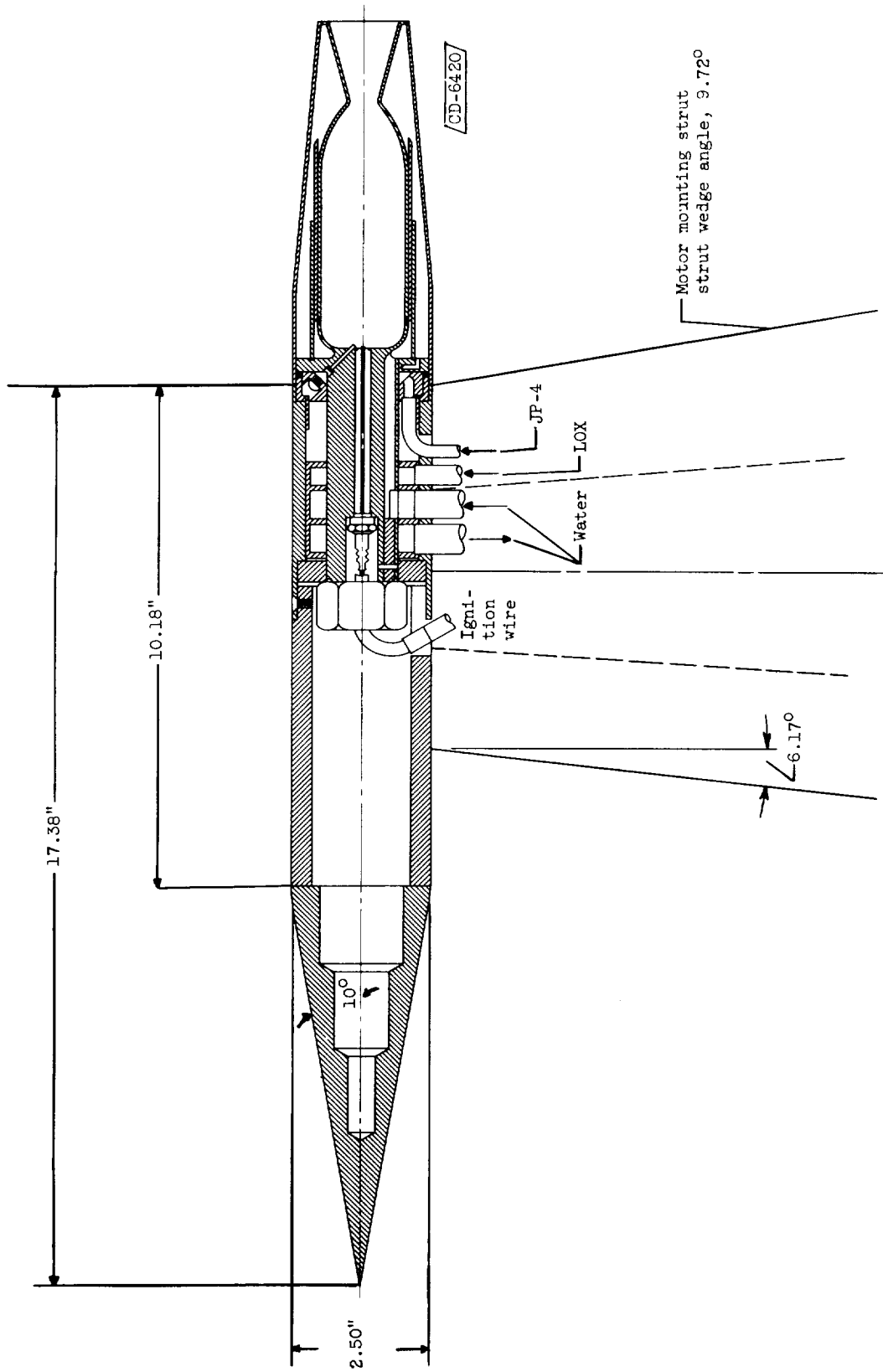
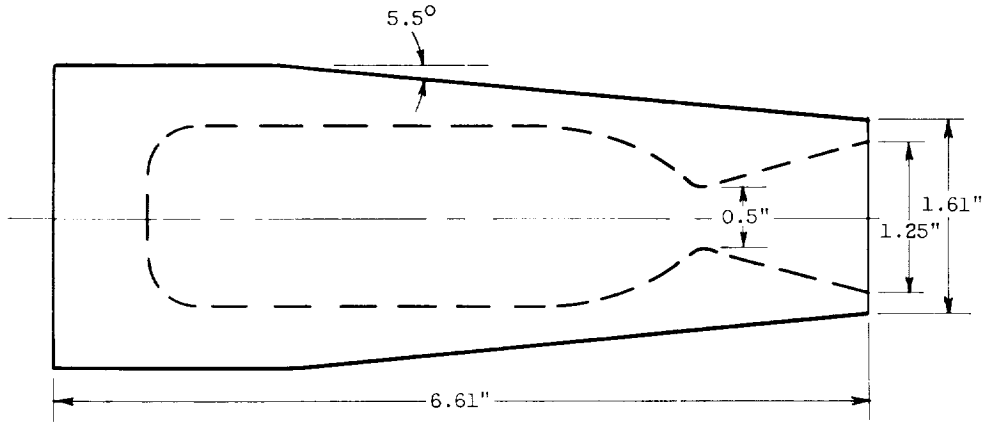
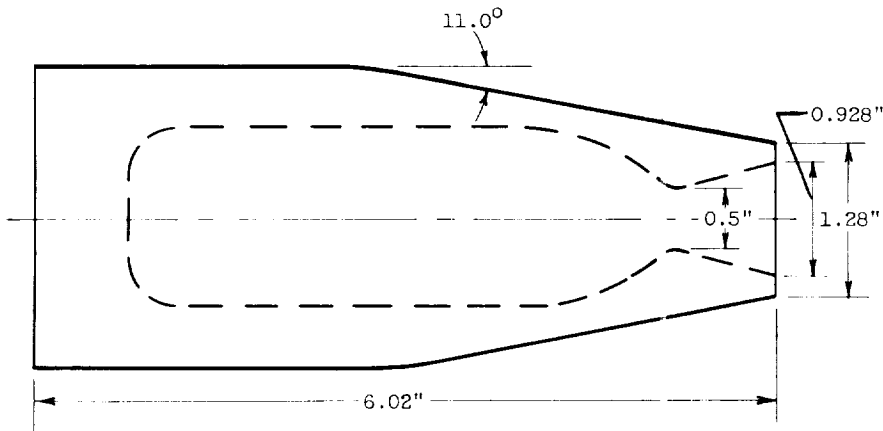


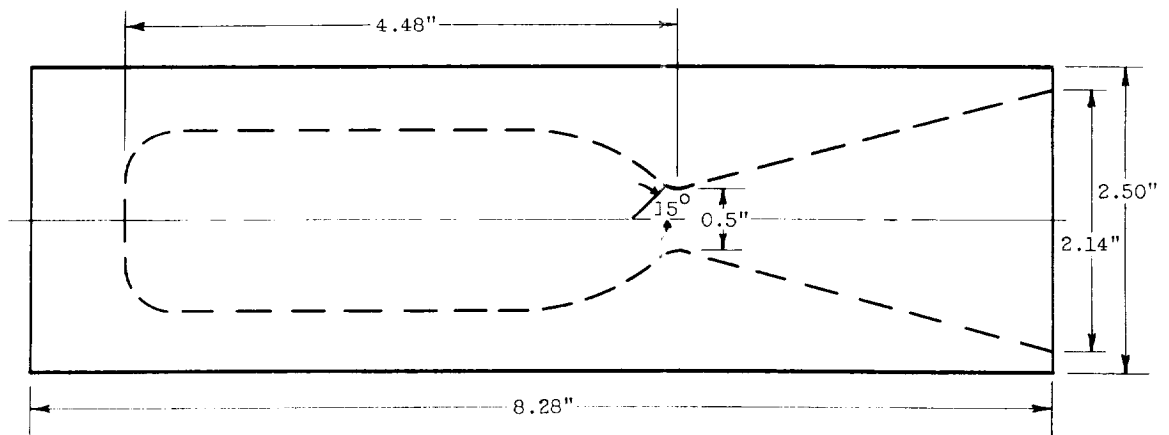
Figure 1. - Typical rocket motor.



(a) Area ratio, A_e/A_t , 6.25.



(b) Area ratio, A_e/A_t , 3.44.



(c) Area ratio, A_e/A_t , 18.31.

CD-6419

Figure 2. - Rocket motor configurations.

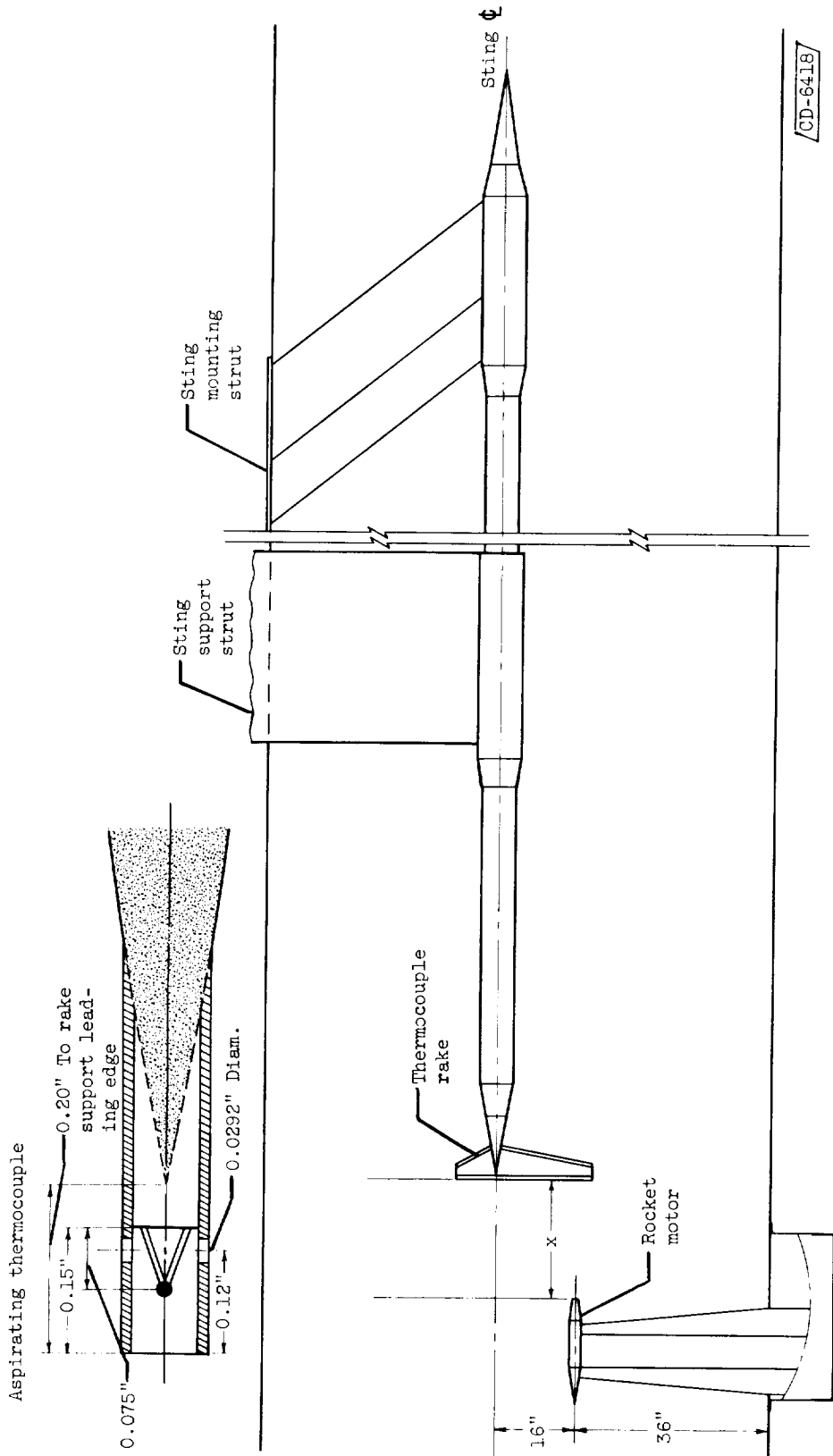
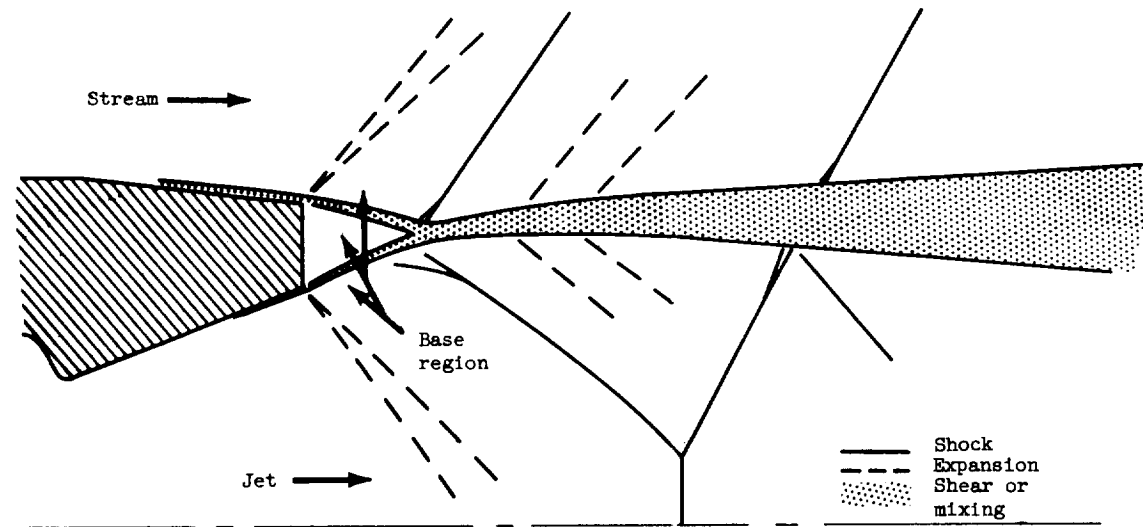
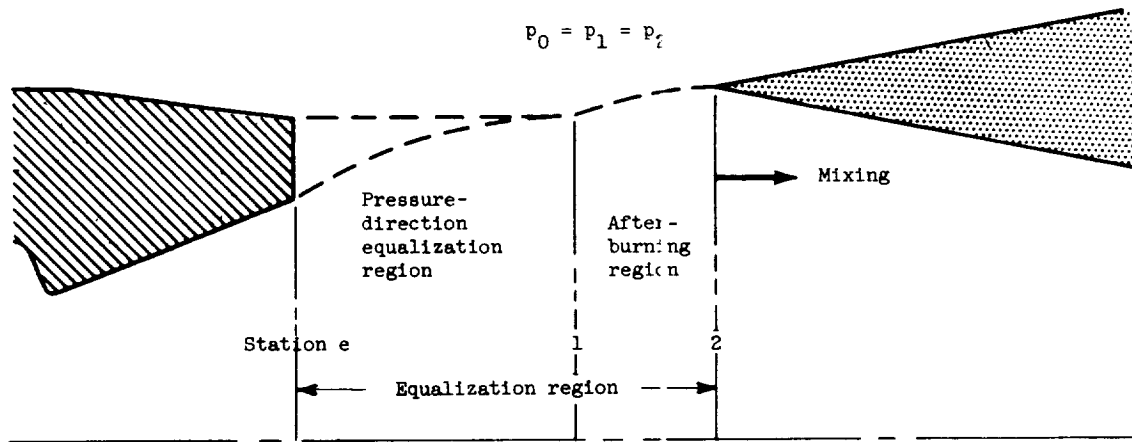


Figure 3. - Installation in 8- by 6-foot wind tunnel.



(a) Actual equalization.



(b) Idealized equalization.

Figure 4. - Jet-stream pressure- and flow-direction equalization.

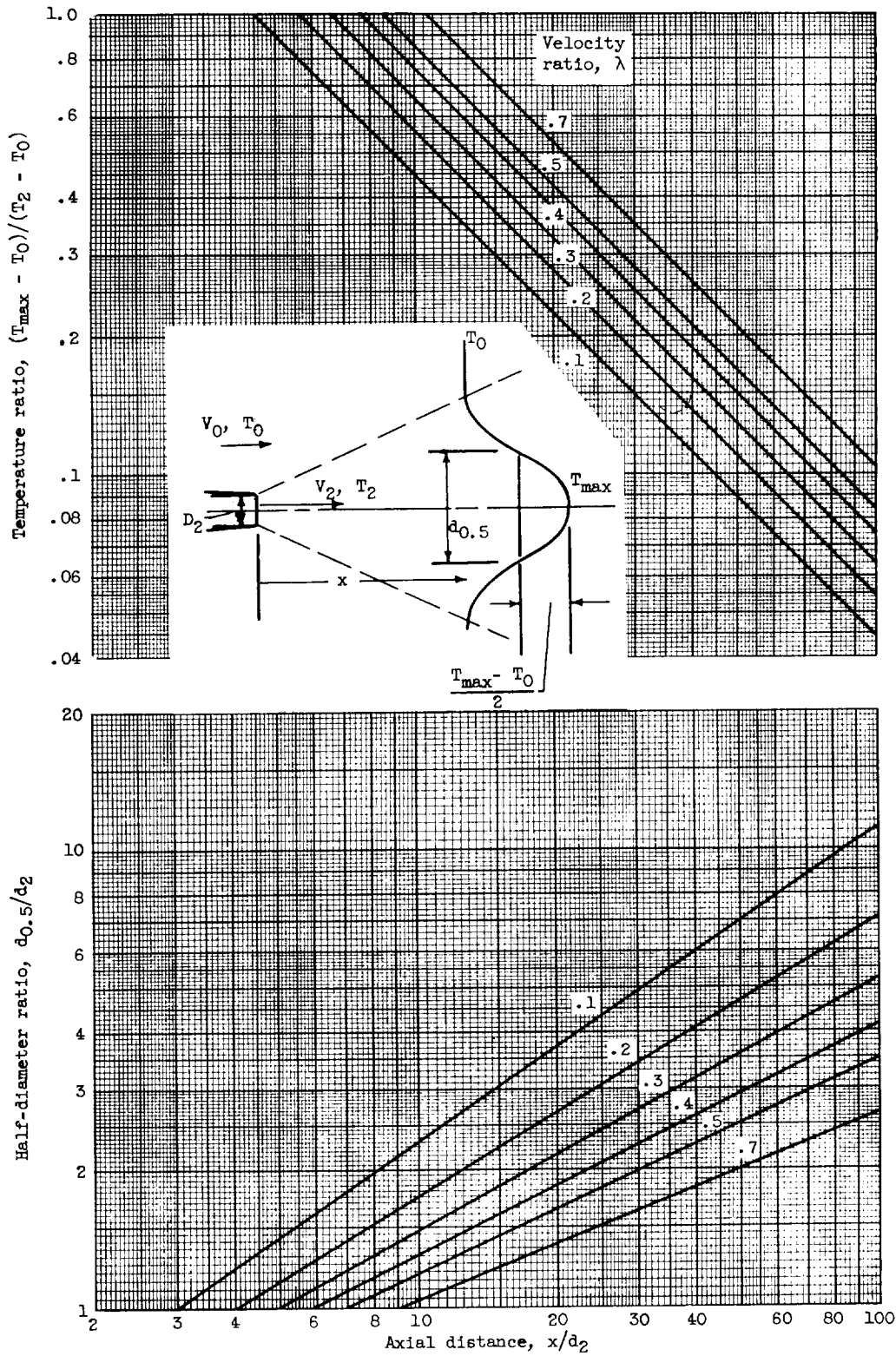


Figure 5. - Low-speed spreading curves (from cross plots of concentration data of ref. 4).

$$\text{—————} \quad \frac{T - T_0}{T_{\max} - T_0} = \frac{1}{2} \left(1 + \cos \frac{\pi}{2} \frac{r}{r_{0.5}} \right)$$

..... Experimental data

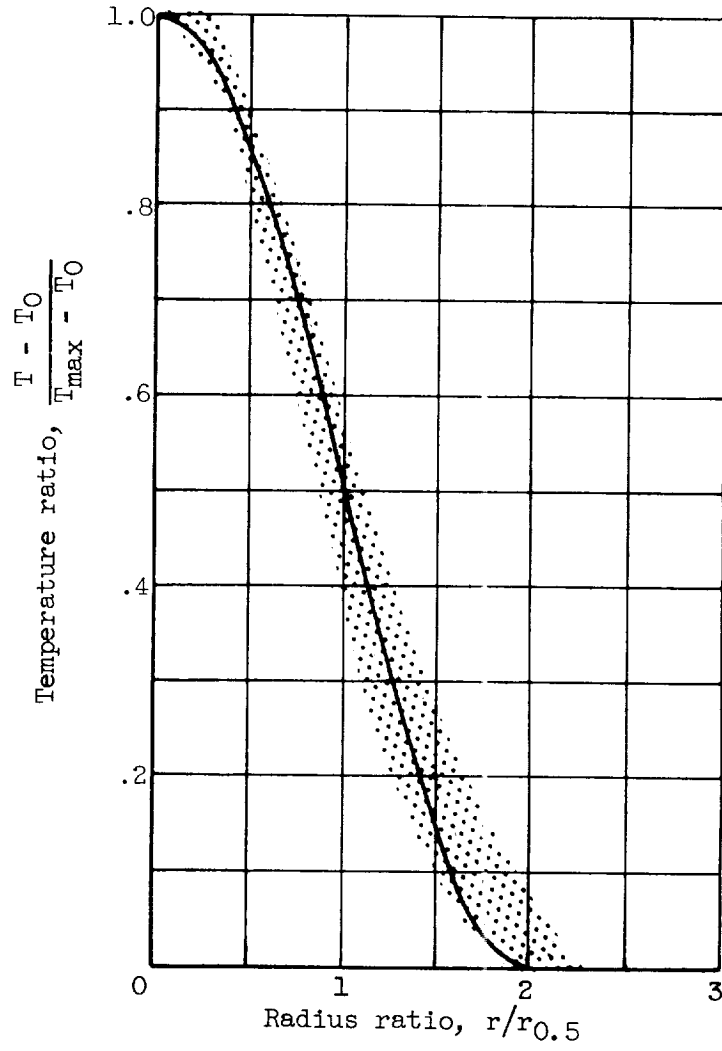
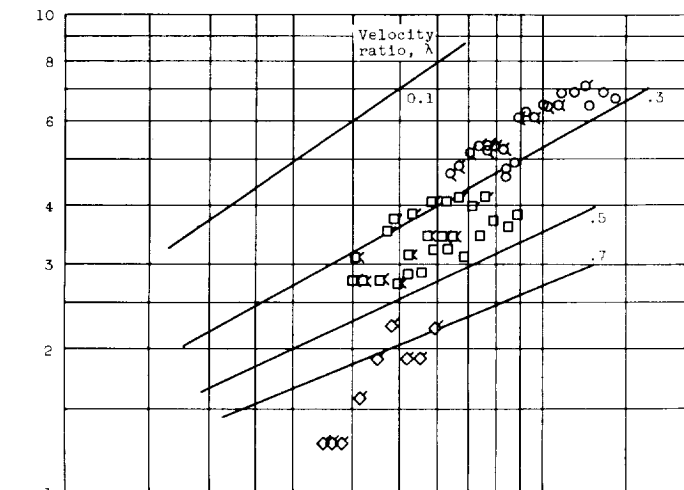
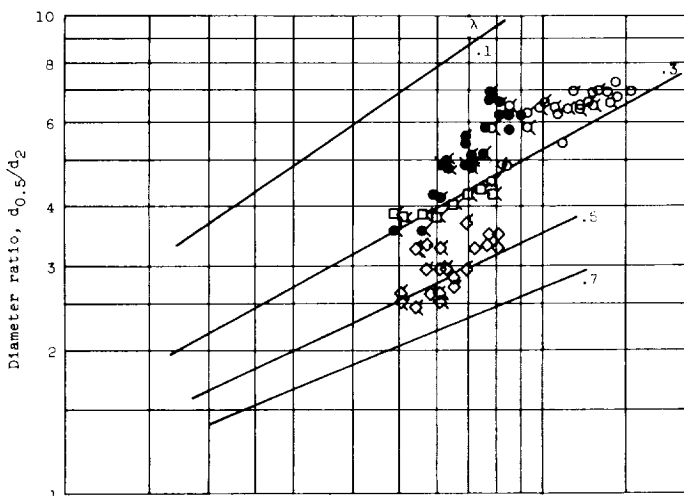


Figure 6. - Temperature profile.



(a) Area ratio, A_p/A_t , 3.44.

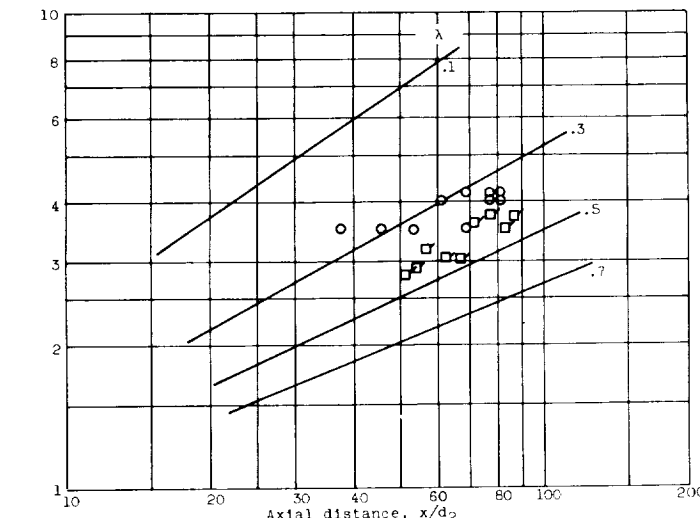
Run	M_0	P_0 , lb/sq in. abs	η	λ
1	0.8	300	0.346	0.19
2		400	.531	.19
3		480	.386	.22
4	1.5	300	.761	.31
5		400	.781	.31
6	2.0	530	.840	.30
7		400	.709	.41



(b) Area ratio, A_p/A_t , 6.25.

Run	M_0	P_0 , lb/sq in. abs	η	λ
8	0.8	300	0.189	0.31
9		400	.257	.26
10		480	.231	.23
11	1.5	470	.296	.43
12	2.0	300	.255	.58
13		430	.311	.52
14		480	.322	.52

Solid symbols indicate sting support strut in fore position



(c) Area ratio, A_p/A_t , 18.31.

Run	M_0	P_0 , lb/sq in. abs	η	λ
15	1.5	400	0.595	0.31
16f	1.8	300	.570	.26

Figure 7. - Jet spreading. Assumed afterburning ratio, τ , 1.0 ($d_1 = d_2$). (Curves from fig. 6.)

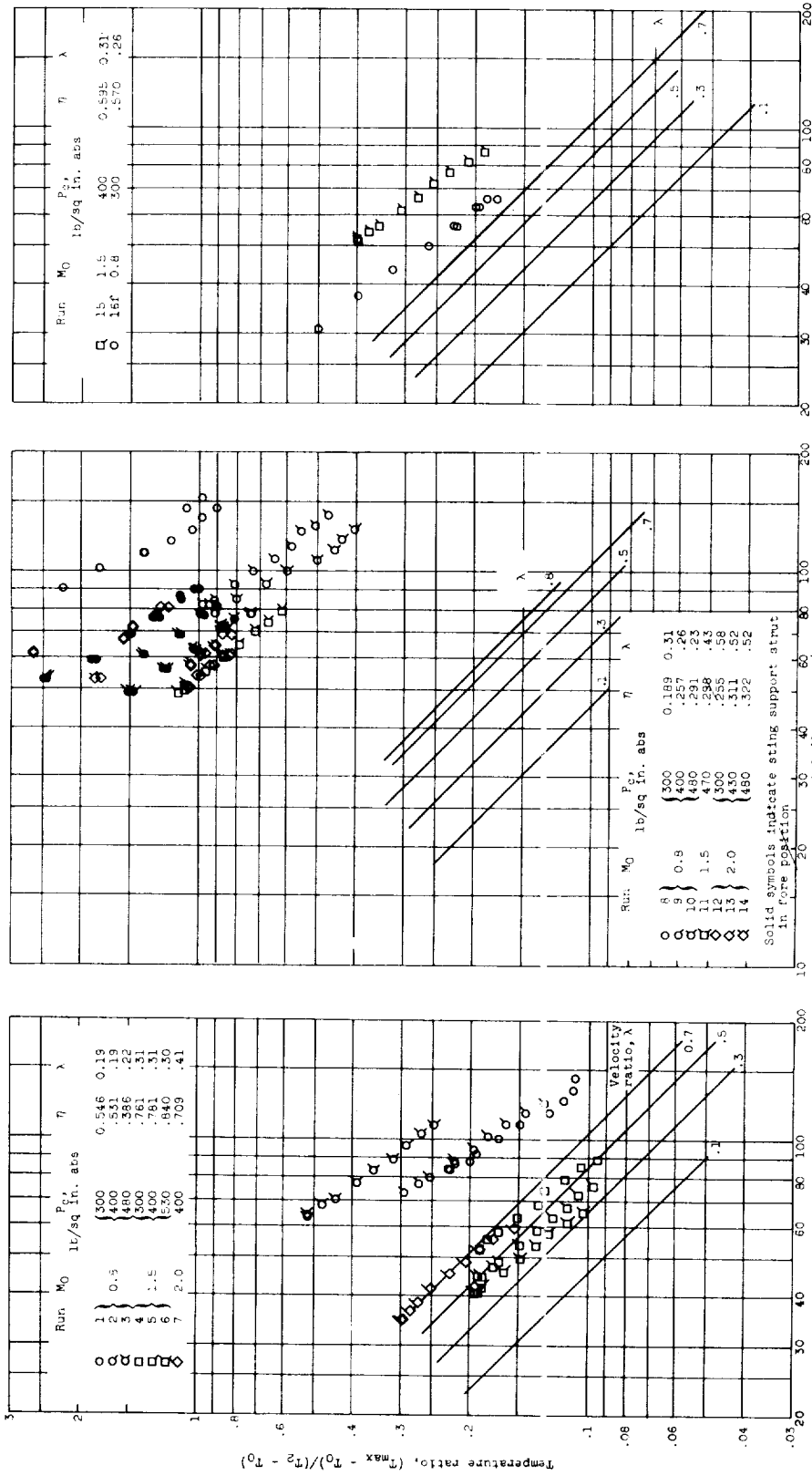


Figure 8. - Temperature decay. No afterburning correction ($r = 1.0$, $T_2 = T_1 = T_c$, $d_1 = d_2$).

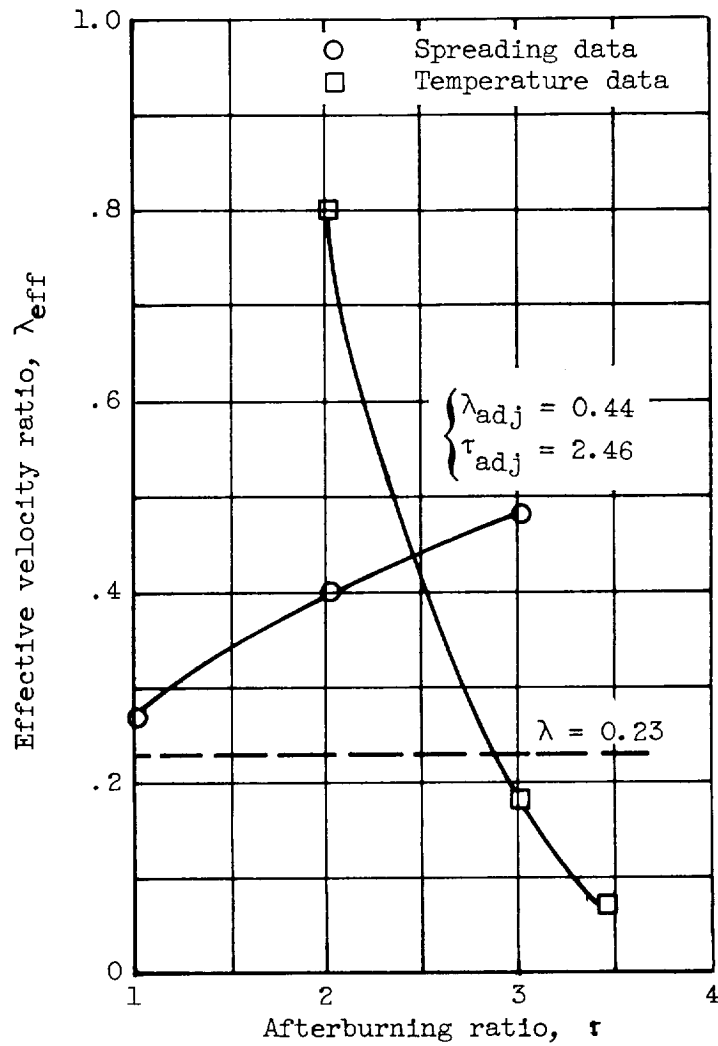
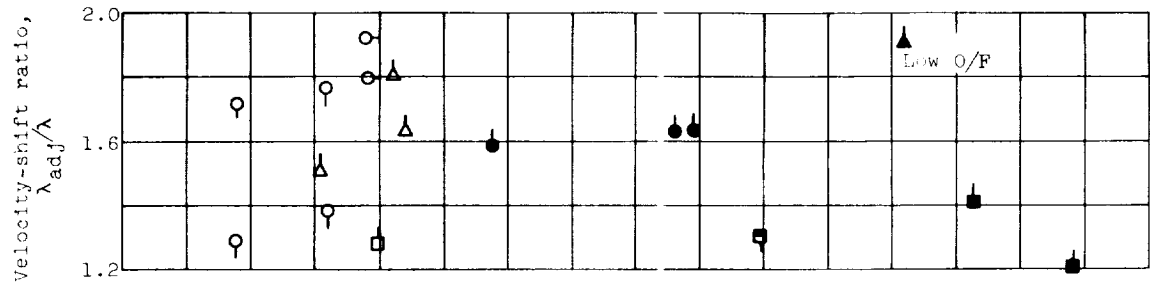
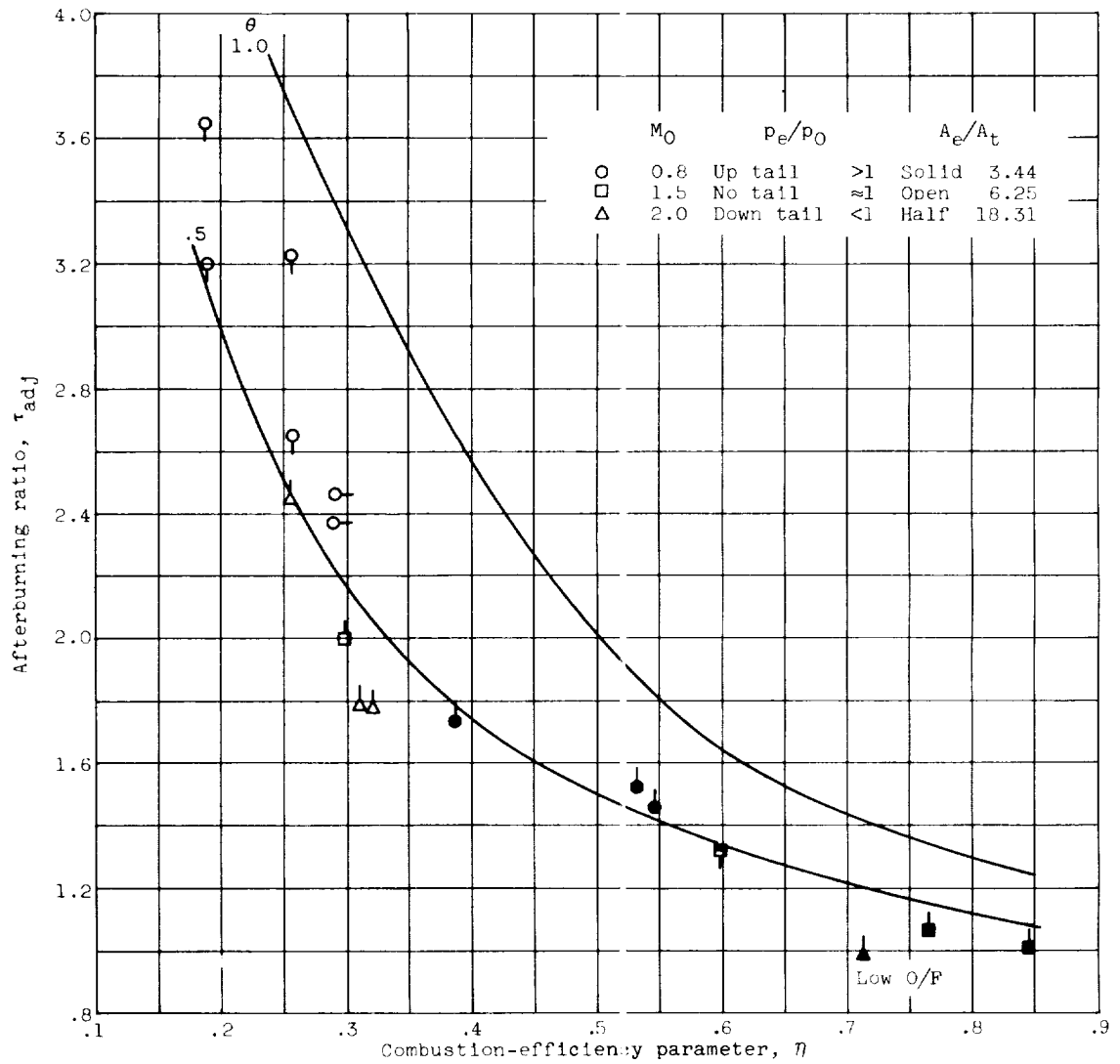


Figure 9. - Typical variation of effective velocity ratio with afterburning ratio. Run 10: $A_e/A_t = 6.25$; $M_0 = 0.8$; $\lambda = 0.23$; $\lambda_{\text{adj}}/\lambda = 1.91$.



(a) Velocity-shift parameter.



(b) Afterburning parameter.

Figure 10. - Summary of adjusted velocity-shift and afterburning ratios.

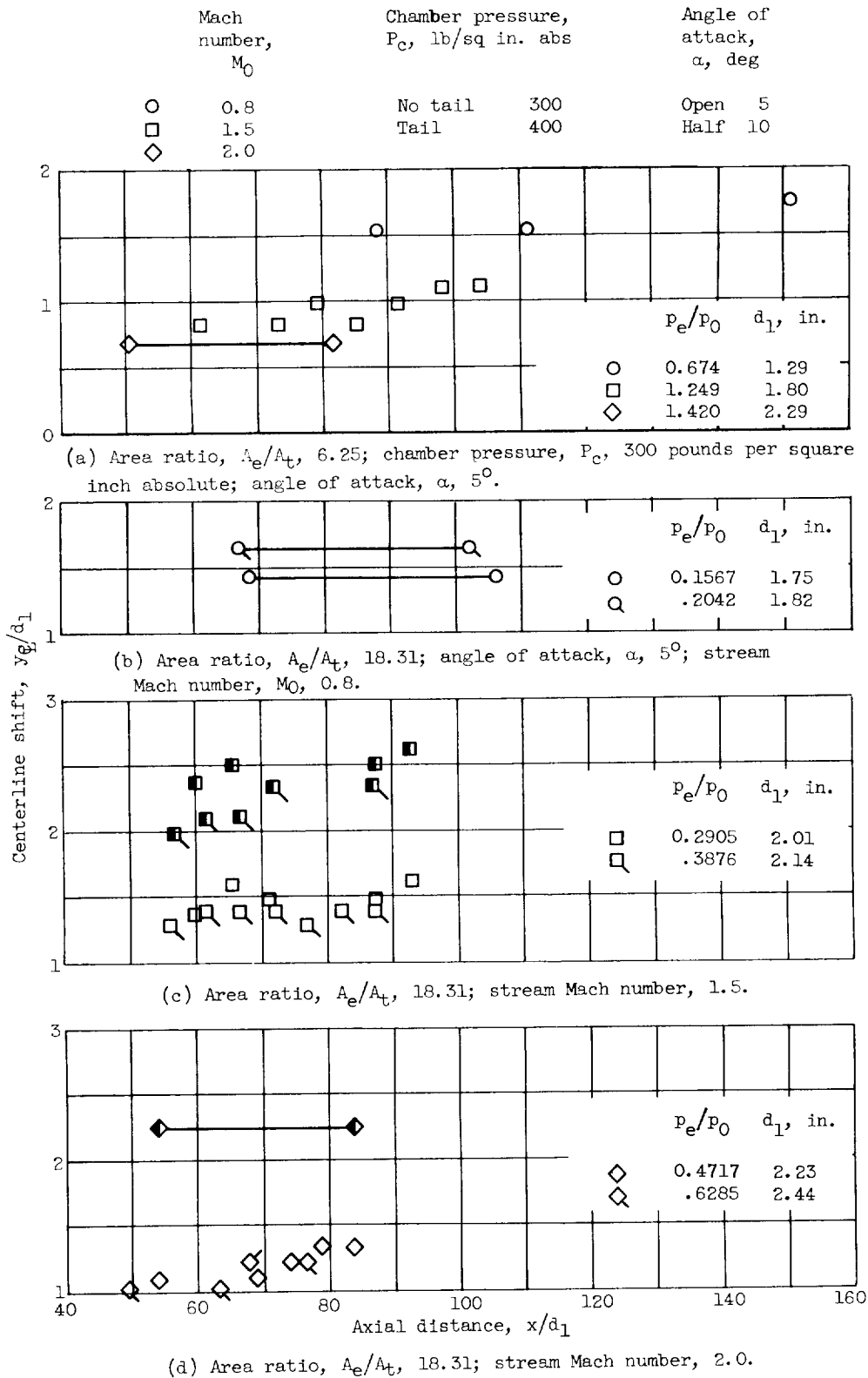


Figure 11. - Jet centerline shift.

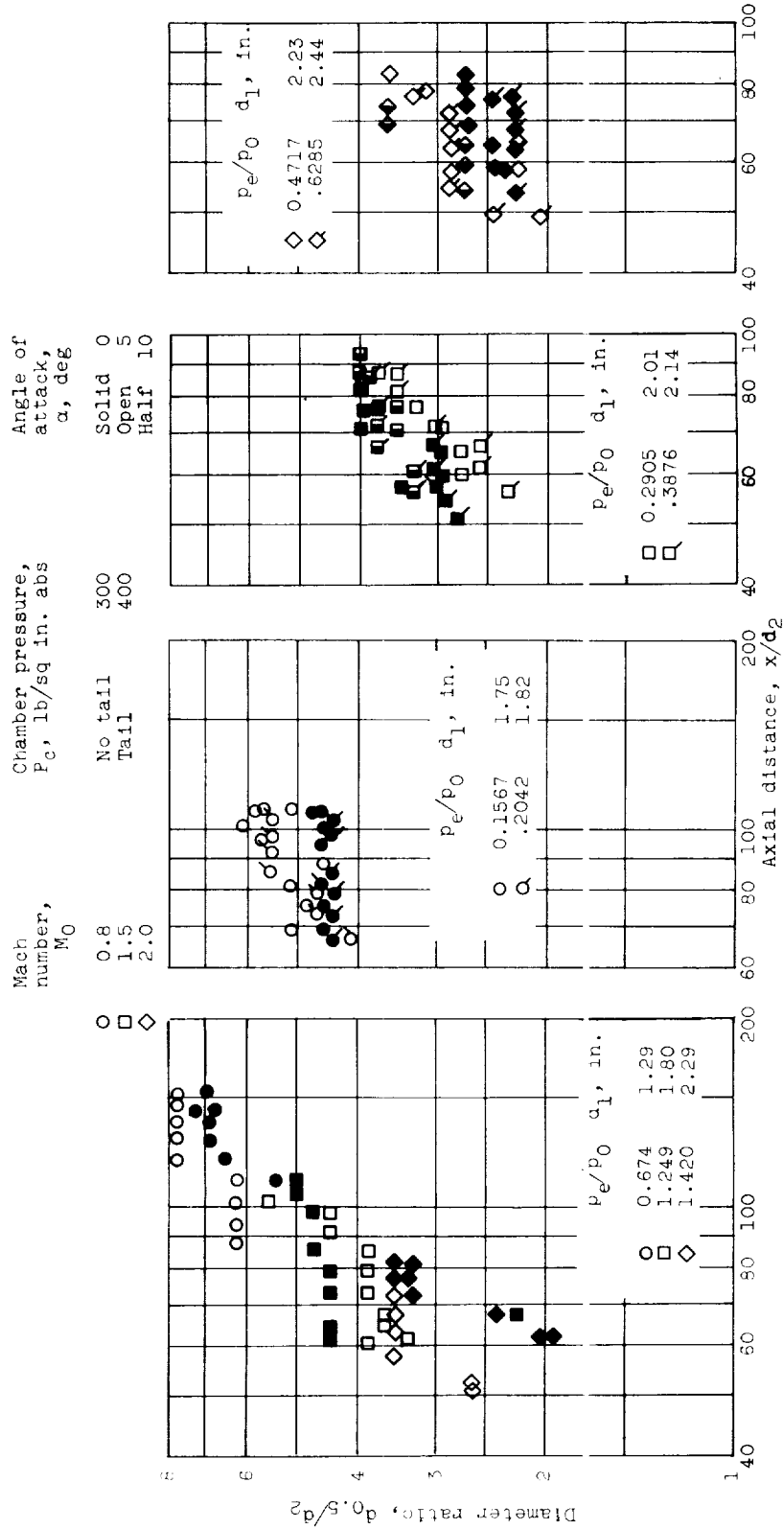


Figure 12. - Jet spreading at angle of attack ($\tau = 1.0$, $d_1 = d_2$).

